Miniaturized optoelectronic tweezers controlled by GaN micro-pixel light emitting diode arrays

Alicja Zarowna-Dabrowska[1,2], Steven L. Neale[2], David Massoubre[1], Jonathan McKendry[1], Bruce R. Rae[3], Robert K. Henderson[3], Mervyn J. Rose[4], Huabing Yin[2], Jonathan M. Cooper[2], Erdan Gu[1*] and Martin D. Dawson[1]

1 Institute of Photonics, University of Strathclyde, Glasgow, UK
2 School of Engineering, University of Glasgow, UK
3 Institute for Integrated Micro and Nano Systems, Joint Research Institute for Integrated Systems, The School of Engineering, University of Edinburgh, UK
4 Electronic Engineering and Physics, University of Dundee, UK
erdan.gu@strath.ac.uk

Abstract: A novel, miniaturized optoelectronic tweezers (OET) system has been developed using a CMOS-controlled GaN micro-pixelated light emitting diode (LED) array as an integrated micro-light source. The micro-LED array offers spatio-temporal and intensity control of the emission pattern, enabling the creation of reconfigurable virtual electrodes to achieve OET. In order to analyse the mechanism responsible for particle manipulation in this OET system, the average particle velocity, electrical field and forces applied to the particles were characterized and simulated. The capability of this miniaturized OET system for manipulating and trapping multiple particles including polystyrene beads and live cells has been successfully demonstrated.

OCIS codes: (230.3670) Light emitting diodes; (230.3990) Micro-optical devices; (230.0250) Optoelectronics; (230.6046) Smart pixel systems; (350.4855) Optical tweezers or optical manipulation; (170.1530) Cell analysis

References and links

1. H. Xie, D. S. Haliyo, and S. Regnier, "A versatile atomic force microscope for three-dimensional nanomanipulation and nanoassembly," Nanotechnology **20**, 215301 (2009).
2. D. J. Stevenson, F. Gunn-Moore, and K. Dholakia, "Light forces the pace: optical manipulation for biophotonics," J. Biomed. Opt. **15**, 041503 (2010).
3. R. Pethig, "Review Article-Dielectrophoresis: Status of the theory, technology, and applications," Biomicrofluidics **4**, 022811 (2010).
4. G. Vieira, T. Henighan, A. Chen, A. J. Hauser, F. Y. Yang, J. J. Chalmers, and R. Sooryakumar, "Magnetic Wire Traps and Programmable Manipulation of Biological Cells," Phys. Rev. Lett. **103**, 128101 (2009).
5. Y. Yamakoshi, Y. Koitabashi, N. Nakajima, and T. Miwa, "Yeast cell trapping in ultrasonic wave field using ultrasonic contrast agent," Jpn. J. Appl. Phys. Part 1 - Regul. Pap. Brief Commun. Rev. Pap. **45**, 4712-4717 (2006).
6. P. Y. Chiou, A. T. Ohta, and M. C. Wu, "Massively parallel manipulation of single cells and microparticles using optical images," Nature **436**, 370-372 (2005).
7. S. L. Neale, M. Mazilu, J. I. B. Wilson, K. Dholakia, and T. F. Krauss, "The resolution of optical traps created by light induced dielectrophoresis (LIDEP)," Opt. Express **15**, 12619-12626 (2007).
8. H. Hwang, Y. J. Choi, W. Choi, S. H. Kim, J. Jang, and J. K. Park, "Interactive manipulation of blood cells using a lens-integrated liquid crystal display based optoelectronic tweezers system," Electrophoresis **29**, 1203-1212 (2008).
9. J. K. Valley, A. Jamshidi, A. T. Ohta, H. Y. Hsu, and M. C. Wu, "Operational regimes and physics present in optoelectronic tweezers," J. Microelectromech. Syst. **17**, 342-350 (2008).
10. J. J. D. McKendry, R. P. Green, A. E. Kelly, Z. Gong, B. Guilhabert, D. Massoubre, E. D. Gu, and M. D. Dawson, "High-Speed Visible Light Communications Using Individual Pixels in a Micro Light-Emitting Diode Array," IEEE Photonics Technol. Lett. **22**, 1346-1348 (2010).
11. T. Kamei, B. M. Paegel, J. R. Scherer, A. M. Skelley, R. A. Street, and R. A. Mathies, "Integrated hydrogenated amorphous Si photodiode detector for microfluidic bioanalytical devices," Anal. Chem. **75**, 5300-5305 (2003).

12. R. A. Street, *Technology and Applications of Amorphous Silicon* (Springer, New York, 2000).
13. J. K. Valley, S. Neale, H. Y. Hsu, A. T. Ohta, A. Jamshidi, and M. C. Wu, "Parallel single-cell light-induced electroporation and dielectrophoretic manipulation," Lab on a Chip **9**, 1714-1720 (2009).
14. B. R. Rae, K. R. Muir, Z. Gong, J. McKendry, J. M. Girkin, E. Gu, D. Renshaw, M. D. Dawson, and R. K. Henderson, "A CMOS Time-Resolved Fluorescence Lifetime Analysis Micro-System," Sensors **9**, 9255-9274 (2009).

1. Introduction

The ability to manipulate micro-sized objects is essential for numerous cell biology experiments, for example observing cell interactions with other cells or their environment, or in cell sorting. There are many competing micromanipulation techniques being actively researched, including mechanical manipulation using AFM tips [1], optical tweezers [2], dielectrophoresis [3], magnetic traps [4] and acoustic traps [5]. Each technique has distinct advantages and disadvantages, in terms of the degree of force that can be applied or the precision of the particle manipulation. A further, recently developed technique, Optoelectronic Tweezers (OET), uses a light-patterned photoconductive electrode to provide real time control over the positioning of electric fields to achieve the particle trapping and manipulation. In response to a projected light pattern, the local conductivity of the photoconductive electrode is modified, creating non-uniform electric fields in liquid interfacing between the photoconductive electrode and a counter electrode and allowing neutral particles to be manipulated by dielectrophoresis (DEP) [3].

OET has advantages over traditional dielectrophoresis as the field can be repositioned; in addition, more particles can be manipulated individually and in parallel than with AFM, magnetic tweezers or optical tweezers [6]. The OET traps have been compared to optical traps and have found to be 470 times stiffer for a similar light intensity [7]. Furthermore, the optical properties of the particles do not constrain the manipulation. Disadvantages of OET are that it is a 2D force and the trapping is not as strong as with an AFM tip or with magnetic traps. There are also limitations on the liquids that the particles can be suspended in, with the liquid conductivity having to be within a certain range determined by the conductivity of the photoconductor. To date, the light pattern that creates the virtual electrode in an OET device was achieved by using either a Digital Micro-mirror Device (DMD) [6] or using an LCD display [8]. However, these DMD and LCD devices are quite bulky, and have limited prospects for achieving multi-functional embodiments and a miniaturized OET device. In this work, we used complementary metal–oxide–semiconductor (CMOS) controlled gallium nitride micro-pixel light emitting diode arrays (micro-LEDs) to create micro-light patterns and to realize a miniaturized OET device. The functionality and capabilities of this miniaturized OET system in particle and cell manipulations are also demonstrated.

2. The OET device structure and operating principle

A typical OET device comprises two electrodes made of indium tin oxide (ITO) coated borosilicate glass slides which form a sample chamber [6]. The bottom electrode is covered with a layer of photoconductive material, typically amorphous silicon (a-Si:H). A conductive liquid is placed between these electrodes, and the electrodes are connected to an electrical function generator. In the dark, the impedance of the photoconductive layer is higher than the impedance of the liquid between the electrodes and almost all the voltage is dropped across the photoconductive layer. Under illumination, the impedance of the photoconductor drops dramatically and the voltage is transferred into the liquid surrounding the illuminated area. A non-uniform electric field is then generated between two electrodes, creating a DEP force on neutral particles between the electrodes. The magnitude and direction of the DEP forces are determined by the relative permittivity of the particle and the liquid in which it is suspended. Particles with high permittivity relative to the liquid medium experience a force towards the high electric field region, i.e. positive DEP, while particles with lower permittivity experience a force away from the high field region, i.e. negative DEP (Fig.1a). The DEP force is proportional to the electric field gradient and thus reaches its maximum at the edges of the illuminated area where it dominates the particles' motion.

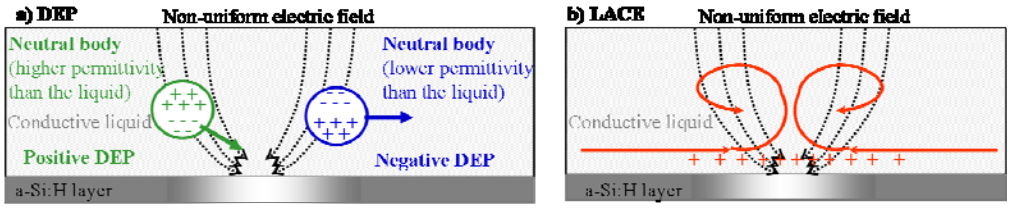

Fig. 1. (Color online) Schematics of a) the dielectrophoresis (DEP) forces generated in OET devices and the resultant particle movement and b) Light-induced AC electro-osmosis (LACE).and induced liquid movement.

In addition, small quantities of ions are suspended in the liquid and they are attracted by the opposite charges appearing at the solid (electrode) surface. When a low frequency AC bias is applied, a force is experienced by the ions at the liquid/solid interface. These ions are driven by the electric-field-induced force which is stronger at the illuminated region of the device. The movement of the ions drags the bulk of the fluid with them. This phenomenon is named light-induced AC electroosmosis (LACE) [9]. This liquid movement towards the illuminated area close to the surface, and away from the illuminated area above it, creates vortices (Fig. 1b). This phenomenon is responsible for particle and liquid movement over relatively large distances (a few millimeters from the illuminated area).

3. Miniaturized OET design and structure

As described above, OET devices rely on the light pattern created on the surface of the photoconductive layer inside the sample chamber. So far, OET devices have employed bulky light sources including lasers and lamps, projected onto a digital micro-mirror device or a video-projector, with the light then coupled into the sample chamber with microscope lenses. The whole setup thus takes up significant space on an optical table. In this work, the size of the optical control and patterning system was considerably decreased by use of CMOS-controlled gallium nitride micro-LEDs as an integrated light source. These sources and their CMOS control have been reported elsewhere [10]. Briefly, they consist of a device chip containing an array of 8 x 8 micro-sized GaN LED pixels on a 200µm center-to-center pitch, flip-chip bonded to a CMOS control backplane. Light is thus extracted through the polished sapphire epitaxial substrate. Local electrical drivers embodied in the CMOS provide direct and *independent* control of the light output of each pixel, which can be operated continuously or in other modes such as nanosecond pulsing [10]. These sources can thus provide a controllable light pattern directly without using a spatial light modulator and offer the possibility of switching modes of operation for e.g. combined particle manipulation and time-resolved fluorescence analysis. We performed our initial investigations of OET using a blue (450nm) device, as described below, but then found a 520nm device to be the most suitable. In both cases, to facilitate pixel size dependent investigations, the respective device chips used consisted of 8 rows of pixels, each of which had a fixed pixel diameter but between which the pixel diameter increased by 10µm intervals (i.e. 14µm row, 24µm row, 34µm row, 44µm row, 54µm row, 64µm row, 74µm row and 84µm row). A typical turn-on voltage for the 450nm devices is 3.0V and they can produce an output power up to 4.5mW per pixel (as measured for an 84µm diameter pixel at a drive current of 140mA) [10]. The 520nm micro-LEDs have a typical turn-on voltage of 4.2V and an average output power of 260µW at 6mA for an 84µm diameter pixel size. This micro-pixellated light source is powered and controlled by a computer through a USB connection.

To create a compact OET device, the micro-LEDs were placed underneath the a-Si:H lower electrode allowing microscope observation of the sample chamber from the top. The spacing between two electrodes, ITO coated glass and a-Si:H – ITO coated glass, was 100µm. In addition, a low-cost lens, 6 mm in diameter and of NA 0.55 (Geltech™, ThorLabs) was fixed on the top of micro-LEDs to focus their light (1:1 image) onto the a-Si:H surface. Figures 2a and 2b show the miniaturized OET system and its schematic arrangement, respectively.

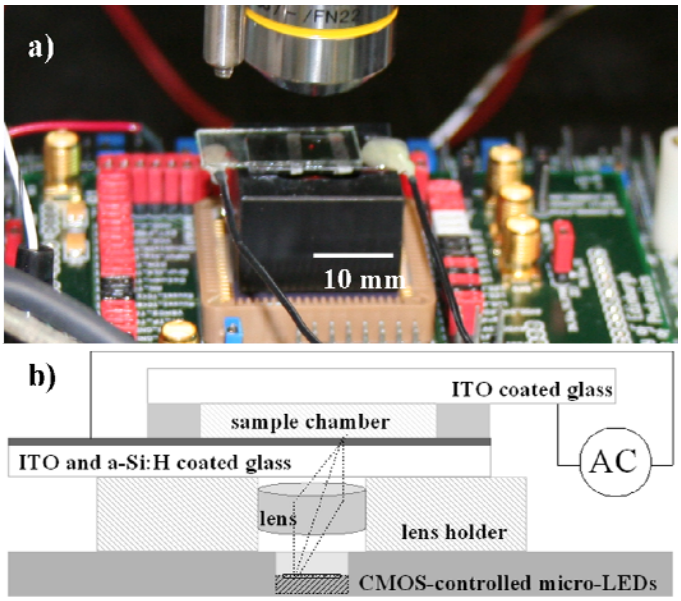

Fig. 2. (Color online) a) Oblique view photograph of the integrated miniaturised OET device under the microscope, and b) the corresponding cross-sectional schematic diagram.

In the visible spectrum, the a-Si:H absorption is lowest at red wavelengths [11], and most probably for that reason red light has been used to create the photoconductive effect in OET devices in previous studies [6, 7]. However, GaN visible LEDs have their best performance at blue and green wavelengths. Previously, 1µm to 2µm thick a-Si:H layers have been used in OET devices, because thinner layers were not free from defects [6]. When we integrated the micro-LEDs with an OET device with a 1µm thick layer of a-Si:H, however, all the light from the blue or green micro-pixels was fully absorbed before it reached the top a-Si:H surface and no DEP effect on the particles was seen. This was due to the absorption of the a-Si:H being up to ten times larger at green wavelengths than in the red part of the spectrum (the absorption coefficient of a-Si:H, α, is 10^4 cm^{-1} at 625nm, and 10^5 cm^{-1} at 520nm), and being even stronger at the 450nm blue wavelength ($5*10^5$ cm^{-1}) [11, 12]. We found, however, that by optimizing the Plasma Enhanced Chemical Vapour Deposition (PECVD), it was possible to produce a high quality 300nm thick a-Si:H layer without defects, and thus to achieve OET using green excitation. The a-Si:H was deposited using a modified DP800 PECVD capacitively coupled system (Oxford Plasma technology) with an electrode of 380mm diameter and 30mm spacing. The lower grounded plate held the patterned ITO glass substrates and was heated to a temperature of 220°C with the upper plate RF driven at 13.56 MHz with an input power of 10 Watts. The silicon growth rate was $0.8As^{-1}$ from pure silane at a flow rate of 75 sccm and a chamber pressure of 100mTorr.

For the trapping experiments, the output voltage (LED bias) of the CMOS driver was fixed at 4.95V for all 520nm wavelength pixels in a row (giving currents of 0.6mA for the 14µm pixel to 6mA for the 84µm pixel). The output optical power density was measured for each pixel size, both at the device and delivered to the photoconductive electrode. Because of size dependent effects, the output power density at each pixel was ~$5W/cm^2$ almost independent of the pixel size, of which 0.4-$0.6W/cm^2$ (calibrated independently in each case) was delivered though the package and lens system to the photoconductive electrode. To achieve particle trapping, a range of parameters related to the OET device operation, such as AC drive frequency, voltage and solution conductivity, have been optimized. We chose 10µm polystyrene beads (Thermo Fisher Scientific, UK) in low concentration KCl solution and Chinese Hamster Ovary cells (CHO-K1 cell line from ATCC) in an isotonic sugar solution (0.3% Dextrose, 8.5% Sucrose in DI water) to demonstrate particle trapping and

manipulation. All chemicals have been supplied by Sigma Aldrich, UK, unless otherwise stated. By using green micro-LED illumination, it was found that the best conditions for particle trapping are: AC frequency of 10 kHz and solution conductivity of 10mSm^{-1} for 10µm polystyrene beads and 1 mSm^{-1} for CHO cells.

CHO cells were cultured at 37 °C and 5% CO_2 in Dulbecco's modified Eagle medium containing nutrient mixture F-12 (DMEM/F12, GIBCO) supplemented with 10% FBS, 2 mM L-glutamine and 100 U/ml of penicillin and streptomycin. Prior to the experiment, cells were put in the suspension. To detach them from the flask surface, cells were treated with 0.25% trypsin solution. After 3 min treatment, DMEM/F12 medium was added to the solution to stop trypsin acting. Next, cells were spun for 3 minutes at 1400rpm, the medium was then aspirated and replaced by sugar solution. The washing procedure was repeated 3 times, to wash off any ions which increase solution conductivity and interfere with trapping. Cell solution at a concentration of 2×10^6 cells ml^{-1} was stored in an eppendorf tube at 4°C prior to the experiment so as to preserve cells. In order to prevent the cell adhesion to the substrate surfaces in the OET chamber, the OET chamber surface has been cleaned thoroughly before adding the cells. With these procedures, our CHO cells did not adhere to the OET chamber surface during the experiment. The viability of CHO cells has been accessed before doing trapping experiment with Trypan Blue stain. A small amount of cells was taken from the main cell solution and stained with 0.01M Trypan Blue. It was confirmed that more than 75% of cells were viable at that stage. The viability of cells in OET devices has been demonstrated in the previous work [13]. That works showed that under the light illumination and electric field strength used in the OET devices, cells remain viable.

4. Results and discussion

Figures 3 and 4 show examples of polystyrene beads and CHO cells, respectively, trapped by pixels of the green micro-LED array (the detailed trapping procedures are shown in supplementary videos S1, S2 and S3). A small amount of the excitation light is transmitted through the a-Si:H and permits the illuminated area to be imaged at the same time as the trapping.

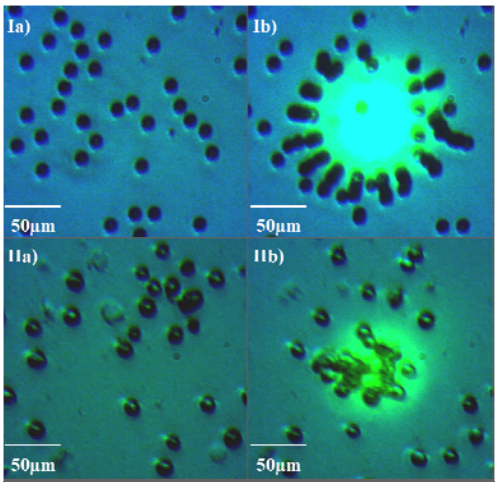

Fig. 3. (Color online) Representative frames of supplementary videos S1 and S2; photographs Ia and IIa were taken with the LEDs turned-off; photographs Ib and IIb were captured 40 seconds after a pixel had been turned on; Ib) Trapping beads with 74µm diameter pixel, at 20V peak to peak voltage (S1 video) IIb) Trapping cells with 54µm pixel at 5V peak to peak voltage (S2 video).

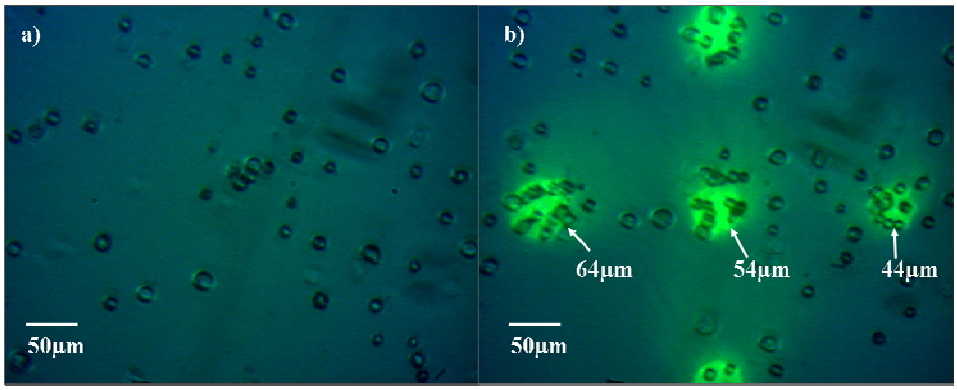

Fig. 4. (Color online) Representative frames of supplementary video S3 showing trapping of cells with 64µm, 54µm and 44µm diameter pixels at 5V peak to peak voltage; photograph a) was taken before any micro-LED has been turned-on; photograph b) was captured after 5 pixels had been turned on.

These images clearly demonstrate that our miniaturized OET device with integrated micro-LED light source is capable of particle/cell manipulation and trapping. Our results also showed that by operating at a relatively low frequency (10 kHz) in a low conductivity liquid (1 or 10 mSm^{-1}), particles and cells could be attracted to the LED pixel from hundreds of microns away. We have further investigated how the cell velocity during the trapping depends on the LED pixel diameter (via the field and field gradient) and AC voltage applied. These results are shown in figure 5.

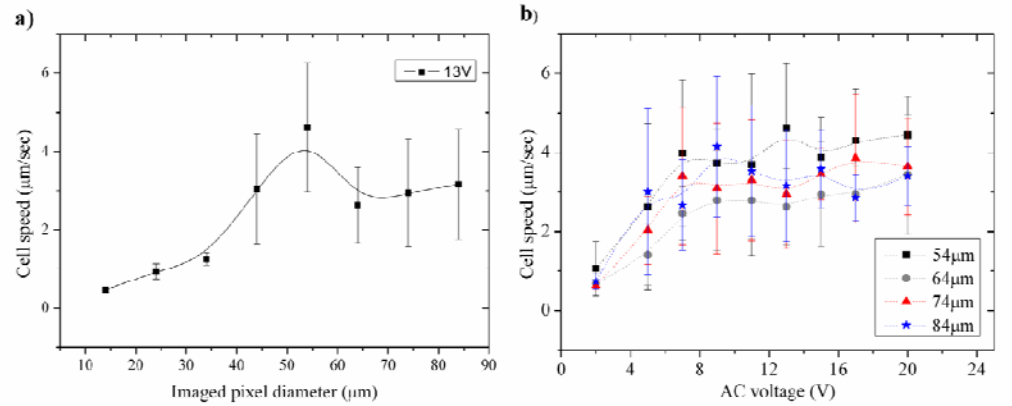

Fig. 5. (Color online) a) A plot of average cell velocity as a function of imaged pixel diameter for one of the AC voltages (13V) applied between the ITO electrodes; b) A plot of average cell trapping as a function of AC voltage for 4 different pixel sizes. Error bars represent +2σ, -2σ.

The time for cells to travel a trapping distance of 150µm was measured and the cell average velocity was then calculated. This cell velocity was evaluated as a function of the diameter of the micro-LED pixel (Fig. 5a) and the AC voltage applied for 4 different pixel sizes (Fig. 5b). The reason for the large error bars in figure 5 is the variation of the cell size (mass) and shape. The results shown in figure 5 provide information on how the average cell velocity changes with LED pixel size and AC bias which enables to find the best conditions for cell trapping. These characterizations cannot be extrapolated from the results of polystyrene beads as the live cell and polystyrene beads have very different physical properties e.g. their permittivity and the trapping mechanisms are also different.

Figure 5a shows the cell velocity increases monotonically with pixel diameter from 14µm to 54µm, reaching a maximum when the 54µm pixel has been used and then, for bigger pixels, the speed is lower, with little increase when the pixel diameter increase from 64µm to 84µm.

Figure 5b shows a roughly linear increase in cell velocity between 0 and 8V followed by little further increase. When comparing the velocities generated by the four biggest pixels for each voltage, in almost all conditions the 54µm diameter pixel generated the highest cell average speed. All pixels generated similar optical power densities; consequently to explain why the 54µm pixel was generating higher speeds required more detailed analysis.

To better understand the trends present, Finite Element Method (FEM) simulations were performed, in which we simulated the forces attracting cells towards the illuminated area. Forces directly influenced cell acceleration and changed the cell trapping speed. As previously discussed, there are two mechanisms which induce the force placed onto the particles, namely Dielectrophoresis and Light Activated AC Electroosmosis. The DEP force is given by Eq. (1);

$$F = 2\pi r^3 \varepsilon_m \,\mathrm{Re}[k(\omega)]\nabla E^2 \qquad (1)$$

where ε_m is the permittivity of the medium, Re[k(ω)] is the Clausius-Mossotti factor and ∇E^2 is the gradient of the electric field squared [3]. To calculate the force due to LACE, the velocity of the ions (the slip velocity) in the liquid was calculated first from Eq. (2);

$$v_{slip} = -\frac{\varepsilon_m \zeta E}{\eta} \qquad (2)$$

Where ζ is the zeta potential, E is the electric field and η is the liquid viscosity [9]. The details of the theory explaining the zeta potential calculation have been presented in previous publications [9]. Once the velocity of the liquid is known, the LACE force on the particle could be calculated by considering the Stokes drag at this velocity, Eq. (3).

$$F = 6\pi\eta R v_{slip} \qquad (3)$$

Where *R* is the radius of spherical objects in [m] [9]. From these equations it can be seen that the DEP force is proportional to the gradient of the electric field squared and the LACE force is directly proportional to the electrical field. Consequently, simulations of electrical field and the square of the electrical field gradient have been performed in order to compare the DEP and LACE forces.

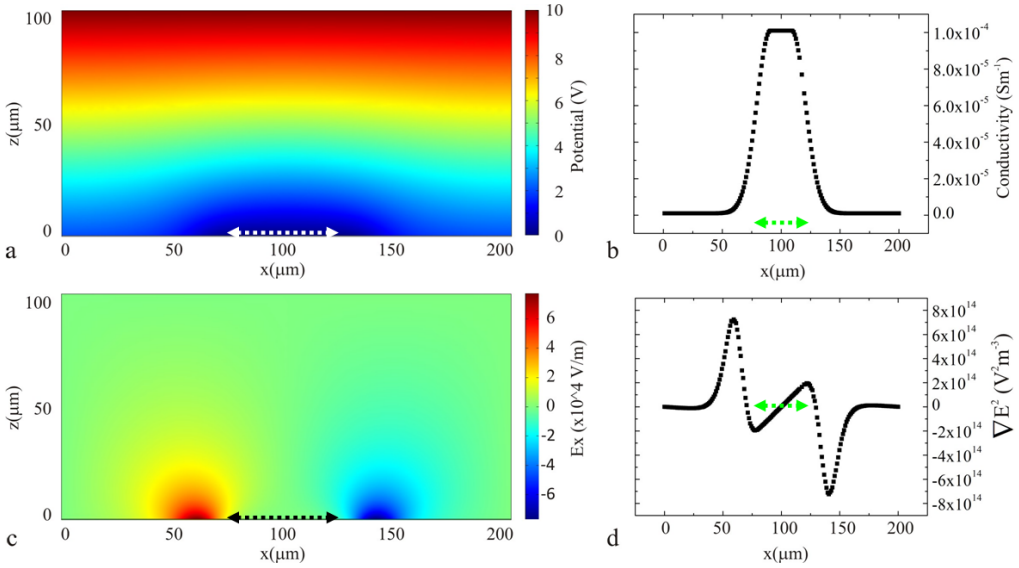

Fig. 6. (Color online) Results of the simulations with schematic of illuminated area (the two-headed arrow dashed lines indicate the pixel imaged spot diameter and position in each case): a) the liquid above the a-Si:H is simulated and the potential dropped across it is shown (100µm

is the real distance between the two electrodes), b) the conductivity of the a-Si:H as a function of position is shown, similar to the intensity profile; c) the electric field distribution is in the x direction, d) the gradient of the electric field squared in the liquid just above the a-Si:H.

Figure 6a shows the results of simulations performed (COMSOL Multiphysics) of the a-Si:H and the potential drop in the liquid above the a-Si:H in the OET device. The simulations use the quasi-static approximation which in this case is valid as the device is much smaller than the wavelength of the AC field being applied [9]. The optical intensity profiles of the four largest micro-LEDs were measured at the a-Si:H and were found to fit well to a profile of two Gaussian distributions with a flat top between them. It was assumed [9] that the conductivity of the a-Si:H would increase linearly with the optical intensity and so conductivity profiles similar to the intensity profiles were put into the simulations (shown in Fig. 6b). The magnitude of the conductivity was taken at $1x10^{-6}$ Sm^{-1} for the dark a-Si:H and $1x10^{-4}$ Sm^{-1} for the illuminated a-Si:H (this corresponds to a light intensity of $0.5W/cm^2$ [9]). This resulted in the electric fields in the x direction shown in figure 6c and the gradient of the electric field squared shown in figure 6d. From these simulations, the forces due to DEP and LACE were calculated and are shown in figure 7.

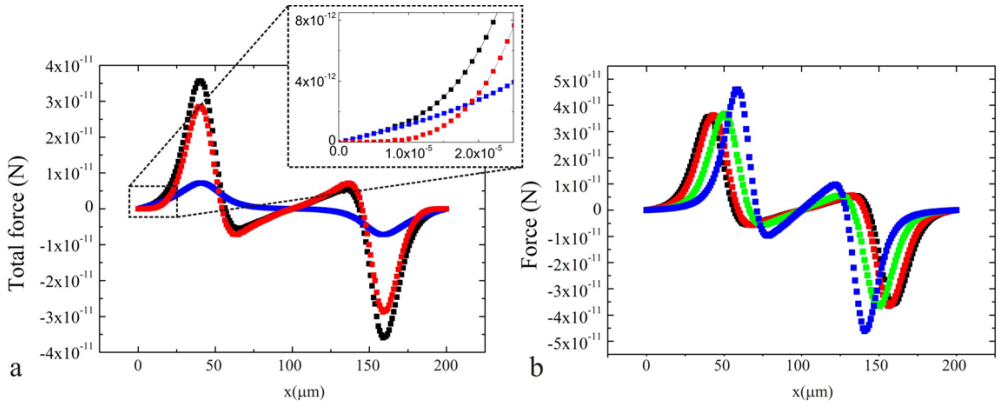

Fig. 7. (Color online) a) The forces due to DEP (red), LACE (blue) and the total force (black) for the 84μm pixel are plotted against position (1-D) on the electrode, the insert shows higher resolution near the origin, where the y axis is in Newtons and the x axis in meters, b) the total force profiles for four pixels are shown - 84μm (black), 74μm (red), 64μm (green) and 54μm (blue).

Figure 7a shows, in the representative example of an 84μm diameter imaged pixel, the forces due to DEP and LACE and the total force. The insert shows a magnified section from the left showing that the LACE force dominates at a large distance from the optical spot and DEP dominates closer to the optical spot. Figure 7b shows that the force profiles created by the three largest pixels, 84 μm, 74 μm and 64 μm, are very similar but the 54μm pixel generates a higher force. The optical intensity profiles of the all four LED pixels had varying widths but the Gaussian decrease in intensity at the sides of the three largest were similar. The optical profile of 54μm diameter pixel was sharper, and fitted a thinner Gaussian, producing this larger force. As described before, we have observed experimentally that the three largest micro-LEDs, 84 μm, 74 μm and 64 μm, were not attracting cells stronger than a 54μm diameter pixel (results in Fig. 5a) and the speed generated by them was lower than that generated by 54μm pixel. This agrees with the simulation results.

For this first miniaturized OET device controlled by CMOS-driven GaN micro-LEDs, the possible maximum power output has been limited by the imaging optics and the particular CMOS chip used. The current CMOS could not provide voltages higher than 5V. The typical turn on voltage of 520nm micro-LEDs was 4.2V and consequently the higher optical powers available from the bare micro-LEDs have not been used. The next generation CMOS driver currently being tested will allow us to drive at higher voltages (up to 7V) and scale the array

to 16 x 16 individually driven elements on a pitch of 100μm. Further work will focus on employing these and even smaller pitch LEDs allowing easy movement between pixels, and on performing time-resolved micro-fluorescence measurements *in situ* [14] for a multi-function trapping and measurement system.

5. Conclusion

In summary, by using a CMOS-controlled 520nm GaN micro-pixelated LED array as an integrated micro-light source, we have developed a miniaturized optoelectronic tweezers system. With the resulting high spatio-temporal and intensity control, the emission pattern generated from the micro-LED array is capable of creating reconfigurable virtual electrodes to achieve miniaturized OET. We have characterized and simulated the average particle velocity, electrical field and forces applied to the particles in this system. Our measurements show the average cell velocity increases with increasing micro-LED pixel diameters from 14 to 54μm and then saturates afterwards. The simulation indicates that the LACE force dominates when the particles are far away from the LED pixel whereas DEP force is much stronger at a short distance.

The capability of this miniaturized OET system for manipulating and trapping multiple particles including polystyrene beads and live cells was successfully demonstrated. This technique has significant potential to develop portable and low-cost instruments for high throughput manipulation and detection of biological particles.

Acknowledgements

This work was funded under the Scottish Consortium on Integrated Microphotonic Systems and by EPSRC under the HYPIX program. SLN thanks the Royal Academy of Engineering for support under a personal research fellowship.

Supporting information available

Videos recorded by a CDD camera at 10 frames per second are provided. Video S1 show 10μm polystyrene beads being attracted by a 74μm diameter pixel, at 20V peak to peak voltage and has been accelerated five times. Video S2 shows CHO cells being attracted by 54μm pixel at 5V peak to peak voltage and has been accelerated two times. Video S3 shows trapping of CHO cells with 64μm, 54μm and 44μm pixels at 5V peak to peak voltage and has been accelerated five times.